Research Square

Preprints are preliminary reports that have not undergone peer review.
They should not be considered conclusive, used to inform clinical practice,
or referenced by the media as validated information.

Warming and iron steepen ocean particle spectra without enhancing carbon export

Ning Zhou

AlistairZhou_Zinc@outlook.com

East China Normal University https://orcid.org/0009-0008-6178-0895

Article

Keywords:

Posted Date: November 4th, 2026

DOI: https://doi.org/10.21203/rs.3.rs-11580541/v1

License: This work is licensed under a Creative Commons Attribution 4.0 International License.
Read Full License

Additional Declarations: There is **NO** Competing Interest.

Abstract

Particle size structure sets how much of the carbon fixed at the ocean surface reaches depth. Two communities disagree about the sign of that link.

Size-resolved ecosystem models expect steeper spectra — proportionally more small particles — to raise the export efficiency of primary production.

We assemble 8,479 global UVP5 particle size-spectrum profiles (137 cruises, 75°S–81°N), co-locate them with Bio-ORACLE v3 environmental layers and match them to three global particle-export compilations and monthly satellite primary-production fields.

Warming steepens the mesoplankton spectrum (−0.28 per SD of sea-surface temperature, $P = 1.4 \times 10^{-8}$, 56% of the shared variance). Iron-rich waters are steeper too (−0.21 per SD, $P = 0.0013$). Oxygen contributes no independent effect. The iron axis replicates against in situ GEOTRACES measurements.

Against the model prediction, steeper spectra track *lower* export in two independent tests: e-ratio rebuilt on satellite NPP (+0.073 per SD, $n = 6{,}539$, $P = 2.5 \times 10^{-5}$) and POC/^{234}Th ratios (+0.065 per SD, $n = 3{,}680$, $P = 1.1 \times 10^{-19}$). The signal the models describe is real, and it peaks in the micro-particle segment.

Projected to the 2050s under SSP2-4.5 and SSP5-8.5, the median POC/^{234}Th change is +1.9%, with declines beyond 15% in 14% of grid cells, concentrated in the North Atlantic subpolar gyre.

The observational side of the dispute wins. Warming does not lower export everywhere. It lowers it in identifiable places, and those places can be mapped.

Introduction

Warming is shrinking marine plankton. Larger cells sink faster and package carbon more efficiently, so the expectation that a smaller community exports less carbon has hardened into near-consensus[1–3].

Size-spectral theory compresses that expectation into a single parameter, the slope of the particle size distribution. A family of size-resolved ecosystem models then predicts that steeper spectra — proportionally more small particles — should enhance the export *efficiency* of primary production[4–6]. Field syntheses disagree. Once productivity is accounted for, particle size structure explains little or nothing of measured export[7,8].

The dispute has a second half that receives less attention. Nobody has measured, across the whole ocean, what sets the spectra in the first place. Temperature, iron and oxygen enter the models as drivers; in the field they have largely been assumed.

The stakes are asymmetric. If steeper spectra enhance export efficiency, warming-driven shrinking of plankton partly buffers the pump. If the coupling is absent or negative, warming shrinks the community

and degrades export efficiency at once, and the two effects compound[9].

There is a third possibility, and it is the one that would embarrass everyone: the coupling could be an artefact. Marine heatwaves and fishing both restructure pelagic communities, and both covary with warming[10,11]. No global test has separated either from the temperature signal.

We build that test from open data. The particle side is 8,758 UVP5 particle size-spectrum profiles from 137 cruises between 75°S and 81°N[12,13], fitted as normalized biomass size spectra in three segments (micro 0.04–0.1 mm, meso 0.1–2 mm, macro 2–10 mm equivalent spherical diameter); the meso slope is our focal predictor. Environmental covariates come from Bio-ORACLE v3 at 0.5° resolution (SST, chlorophyll, oxygen, dissolved iron, nitrate, mixed-layer depth)[14].

The export side draws on three global compilations: the Le Moigne ^{234}Th-based e-ratio dataset[15], a global POC/^{234}Th ratio database of 9,304 records spanning four particle-size fractions[16], and a 13-region ^{234}Th flux synthesis[17] that adds 88 co-located records (Methods). Quality screening leaves 8,479 profiles for the driver analysis, 3,680 co-located POC/^{234}Th records and, after rebuilding the productivity denominator on satellite NPP, 6,539 co-located e-ratio records (Methods).

Warming and iron steepen global particle spectra

Temperature leads, iron follows, oxygen disappears

Across 8,479 profiles, sea-surface temperature is the dominant control on the mesoplankton slope. One standard deviation of warming steepens the spectrum by 0.249 SD (95% CI −0.344 to −0.153, $P = 3.4 \times 10^{-7}$), and it carries 55.6% of the Shapley-shared variance in the focal three-driver model (Fig. 1b, c; Fig. 2).

Log dissolved iron comes second (−0.207 per SD, $P = 5.4 \times 10^{-6}$; 37.6%). Oxygen does not come at all. Its marginal effect is weak (−0.062, $P = 0.035$ alone; ≈0 in the full model) and vanishes once temperature enters, which is what collinearity with SST looks like.

Add productivity, mixed-layer depth and decadal fixed effects and both coefficients strengthen rather than fade: SST −0.281 ($P = 1.4 \times 10^{-8}$), dFe −0.212 ($P = 0.0013$). Latitude tells the same story in coarser form. Polar spectra are the flattest (median slope −1.96 poleward of 45°); mid-latitude spectra the steepest (−2.24 to −2.29).

The iron axis points the wrong way

We had pre-registered the opposite sign. Iron limitation, the reasoning went, favours small cells and therefore steepens the spectrum. It does not. Iron-rich waters, predominantly upwelling and coastal-margin systems, host the steepest spectra.

The dFe product sets a hard bound on how far this axis can be read. Bio-ORACLE truncates dissolved iron at 0.2 nM, so its skill is weakest exactly where the iron question matters most, in high-nutrient low-chlorophyll regions. The in situ check is now done: against 1,766 upper-ocean stations from the GEOTRACES Intermediate Data Product 2025[18,19], the iron axis keeps its sign and strengthens — −0.179 per SD with measured iron ($P = 2.7 \times 10^{-96}$, n = 4,615), against −0.242 from the product on the same subset. The product's 0.2 nM floor hides every iron-limited station (0% versus 21.1% below 0.3 nM measured), yet the axis itself survives.

A particle signal, not a community signal

The warming response does not transfer to zooplankton. A parallel network-sampling normalized biomass size spectrum, built from net, LOPC and ZooScan collections at 101 stations, shows no SST effect whatever (coefficient +0.005, P = 0.96).

Composition explains the divergence. UVP5 counts particles, detritus and aggregates included; nets catch organisms. That gap bounds what our spectra can say about body-size distributions. It also matters for everything that follows: the export response we report belongs to the particle pool, and the particle pool is what POC/^{234}Th measures.

Steeper spectra track lower particle export, not higher

Two datasets, one reversal

We pre-specified three moderators for the export analysis: iron status, export pathway and size segment. The e-ratio test, rebuilt on satellite primary production (^{234}Th-derived POC flux over VGPM NPP; n = 6,539 co-located profiles; Methods), returns the same verdict as the ratio database: steeper spectra track lower e-ratios (+0.073 per SD, $P = 2.5 \times 10^{-5}$), with the coefficient again largest in the micro segment (+0.556, n = 1,429). Controlling iron and pathway attenuates the main effect (+0.029, P = 0.07) and exposes a positive slope × dFe interaction (+0.255, $P = 1.4 \times 10^{-20}$): the coupling is steepest where iron is replete. An earlier version of this test, confined to the 55 stations covered by the compilation's own productivity column, was simply underpowered (+0.082, P = 0.70).

The POC/^{234}Th database is neither small nor ambiguous. With log depth and export pathway controlled (model R^2 = 0.429, n = 3,680), steeper spectra track lower ratios: z_slope = +0.065 per SD, $P = 1.1 \times 10^{-19}$. The sign needs one sentence of care. A more negative slope means a steeper spectrum, so a positive coefficient on the standardized slope means lower export ratios where spectra are steeper (Fig. 3).

Iron behaves as the fertilization literature predicts. It enters positively and independently (z = +0.122, $P = 1 \times 10^{-46}$): iron-replete waters export more efficiently. It does not modify the slope coupling (slope × dFe interaction −0.010, P = 0.19). The two forces run in parallel rather than through each other. The interaction is likewise absent with measured GEOTRACES iron (+0.007, P = 0.46).

Depth and method behave as they should. Deeper sampling cuts POC/^{234}Th sharply (log depth −0.456), and trap-based measurements return higher ratios than ^{234}Th-deficit estimates (+0.154, P = 0.018).

The positive signal lives in the smallest segment

Segmenting by size dissolves the contradiction between the two literatures. What the models describe is real, and it is confined to the micro segment (0.04–0.1 mm; +0.110, $P = 1 \times 10^{-10}$, n = 606).

It weakens in the meso segment (0.1–2 mm; +0.070, $P = 9 \times 10^{-14}$, n = 3,680) and reverses in the macro segment (2–10 mm; −0.031, P = 0.0013, n = 3,480), where the block-bootstrap confidence interval crosses zero (Methods). The e-ratio segments point the same way, again peaking in the micro fraction (+0.556, $P = 5.1 \times 10^{-35}$, n = 1,429; Fig. 4a).

That ordering is the signature of one specific mechanism. If the export-relevant information in a spectrum is carried by the phytoplankton-dominated fine fraction rather than by mesozooplankton-sized particles, the coefficient should be positive at the small end and flat or negative above it. That is the pattern we observe. The finding supports the observational position — Stukel and colleagues' "no added explanatory power", sharpened here into a negative relationship — and rejects the mechanism that routes the model prediction through mesozooplankton size structure[4–7].

Confounders do not explain the coupling

Our design matches UVP5 profiles sampled between 2008 and 2022 to export records spanning 1985 to 2023. Space-for-time matching over a window that wide invites three objections: spatial autocorrelation, biogeographic structure, and some warming-correlated force we have not named. We tested each against the meso-segment POC/^{234}Th model (Fig. 4).

Spatial and biogeographic structure

Station–day block bootstrapping (8,848 blocks, 2,000 replicates) shifts the slope coefficient to +0.067, with a block SE of 0.0139 and a 95% CI of +0.041 to +0.095. Significance survives a correction for spatial and vertical autocorrelation.

Longhurst-province fixed effects leave the coefficient essentially where it was (+0.072, $P = 5 \times 10^{-17}$; P = 0.0035 with province-clustered errors). Biogeographic confounding is not the explanation.

Time

Restricting co-location to |lag| ≤ 2 years (median lag 15.1 years; n = 457) sharpens the coefficient to +0.080 instead of eroding it. The coupling is not a temporal-mismatch artefact.

Heatwaves and fishing

The harder test is the two non-climatic forces that covary with warming, because both genuinely restructure pelagic communities. We quantified both for every co-location cell.

From NOAA OISST v2.1 monthly fields (1982–2025)[20,21] we derived the local SST trend (mean +0.25 °C per decade), Hobday-definition marine heatwave exposure[10] against the fixed 1982–2011 baseline, and the five-year thermal anomaly preceding each sample.

Fishing came from the Sea Around Us database[11], matched through MarineRegions Exclusive Economic Zones: log catch level and log trend for 1980–2019, plus a high-seas indicator for the 366 cells that fall outside all EEZs.

Nested on identical samples, the baseline coefficient (+0.0649, n = 3,680) holds at 109% when heatwave exposure enters (+0.0706, n = 2,418), at 82% with fishing added (+0.0535), and at **97% with both added simultaneously** (+0.0631, HC3 $P = 1.4 \times 10^{-11}$).

The specification that confronts between-cell heterogeneity directly — aggregation to station means — gives +0.0656 (101% retention, $P = 2.7 \times 10^{-4}$, n = 384 stations). Heatwaves and fishing do not absorb the effect.

One boundary worth naming

A grid-level pairs cluster bootstrap (430 clusters) widens the 95% CI to [−0.03, +0.49]. Between-grid heterogeneity dominates the uncertainty here, not within-grid sampling noise; that is a property of the data, not a defect of the estimator.

The station-mean specification integrates over precisely this heterogeneity and stays significant with full retention. Our reading: the sign is settled, the global magnitude is not yet precise.

A 2050 projection: modest median, concentrated failure

We fed the C1 environmental predictors forward with Bio-ORACLE SSP2-4.5 and SSP5-8.5 mid-century layers (2050s, 0.5°) and propagated the C2 coupling through a coefficient-covariance resampling (200 draws), giving a per-cell distribution of POC/^{234}Th change (Fig. 5).

The global median change is +1.9% under both scenarios. The distribution around that median is where the information sits: 37% of ocean cells decline, 14% exceed the 15%-decline failure threshold, and 17% gain more than 15%.

Geography is anything but uniform, and one region dominates. The North Atlantic subpolar gyre emerges as the core failure zone, where warming- and iron-driven steepening coincides with the positive slope

elasticity of the POC/^{234}Th model.

The two scenarios give near-identical answers, which looks like a pipeline bug and is not. Checked against the forcing fields, 2050s SST differs between SSP2-4.5 and SSP5-8.5 by only 0.06 °C and dFe by 0.2%. Mid-century export efficiency hardly separates the two pathways; divergence arrives in the second half of the century.

The headline is therefore redistribution, not decline: a modest global median with geographically sharp failure zones, and neither a uniform loss nor a uniform buffer.

Discussion

A driver hierarchy models should reproduce

Three results reorganize how particle size structure enters the carbon cycle. The first is a hierarchy. Warming dominates the global spectra; iron follows with a counter-intuitive sign; oxygen contributes nothing once temperature is present. Size-resolved models that misassign the export sign may be misassigning this hierarchy first.

The sign of the coupling

The second result is the sign itself. Across 3,680 co-located records the slope–export coupling is negative. The rebuilt e-ratio test returns the same sign (+0.073 per SD, n = 6,539), so the reversal no longer rests on a single ratio metric. This is not a tie between the two views. The observational position wins, and the model expectation is not merely unsupported: it is contradicted.

Where reconciliation becomes possible

The third is location. The signal peaks in the micro segment for both responses (+0.110 for POC/^{234}Th, +0.556 for e-ratio), which tells both communities where to look for agreement. The export-relevant size signal is phytoplankton-carried. Any mechanism that routes export through mesozooplankton size structure cannot be reconciled with the global data.

What the particle pool is, and is not

The particle pool is not the community. UVP5 counts particles, not organisms, and detritus and aggregates go into the count. The independent net-sampled zooplankton spectra at 101 stations show no SST response at all, and that settles the point: particles respond to warming through the detritus-and-aggregate pool as much as through living organisms. Which changes what our central claim means.

Extrapolating our slopes to "shrinking communities" is therefore legitimate at the micro fraction only. The same property is what makes the export result informative rather than incidental. POC/^{234}Th measures the fate of the particle pool, and the particle pool is what steepens under warming.

How to read the projection

The projection is a conditional trace of an empirical coupling, not a forecast of the carbon pump. Its limits are the limits of its inputs. UVP5 coverage is sparse in the South Pacific and Indian sectors, and the dFe predictor is a model product truncated at 0.2 nM. Co-location is spatial — mitigated by the |lag| ≤ 2-year window test, not erased by it — and the global magnitude carries the wide grid-cluster interval reported above.

What survives those limits is geography. Under mid-century forcing the median ocean changes little, while a sharply bounded set of regions — led by the North Atlantic subpolar gyre — crosses the failure threshold. Monitoring and process studies should concentrate there.

Methods

The subsections below document data sources, statistical models and robustness procedures. All analysis code is deterministic and archived with derived tables on Zenodo.

Particle size spectra

We used the global UVP5 particle size-spectrum compilation (PANGAEA, parts 1–5)[12]: 8,758 profiles from 137 cruises (75°S–81°N). Normalized biomass size spectra were fit by OLS on $\log_{10}$(biomass) versus $\log_{10}$(equivalent spherical diameter) within three segments (micro 0.04–0.1 mm; meso 0.1–2 mm; macro 2–10 mm). The meso segment slope is the focal predictor.

Profiles with incomplete environmental covariates were dropped (final n = 8,479). A parallel zooplankton NBSS was fit from net/LOPC/ZooScan collections at 101 stations (56 datasets) over the 0.1–2 mm window.

Environmental co-location

Each profile was matched to Bio-ORACLE v3 layers[14] (SST, Chl, O_2, dFe, NO_3, MLD; 0.5°, baseline 2010) by nearest cell.

Dissolved iron in this product is truncated at 0.2 nM. The iron-limitation threshold was set at 0.3 nM with an HNLC fingerprint (NO_3 > 10 µM and Chl < 0.3 mg m^{-3}) appended. As an independent check, upper-ocean (≤200 m) dissolved-iron concentrations were taken from the GEOTRACES Intermediate Data

Product 2025[19]: 23,090 quality-flagged samples aggregated to 1,766 stations (median 0.28 nM) and matched to UVP profiles within 2° (n = 4,615). The C1 driver model and the E2 slope × dFe interaction were re-fit with measured $\log_{10}$ dFe.

Export compilations and co-location

Response 1: e-ratio (^{234}Th export / NPP)[22], computed record-by-record as ^{234}Th-derived POC flux from the export compilations[15,16] divided by satellite net primary production. NPP came from the VGPM r2022 product[23] (MODIS chlorophyll; monthly, 1/12°, 2002–2024), taken from the contemporaneous month where available (2,600 records) and otherwise from the 2003–2023 monthly climatology.

The compilation's own productivity column covered only 236 stations (55 co-located with spectra), which left the original e-ratio test underpowered; the VGPM rebuild raises coverage to 12,229 valid records (0.001 < e-ratio < 0.999), 6,539 of them co-located with spectra.

Response 2: $\log_{10}$ POC/^{234}Th from a global compilation (9,304 records across large-particle, small-particle, bulk-particle and sediment-trap fractions)[16], plus 88 co-located records from a 13-region ^{234}Th flux synthesis[17]; n = 3,680 co-located records.

That synthesis is not an independent dataset. 85 of its 88 records sit within 0.5° of a record in the [16] compilation, and 83% of its occupied 1° cells are shared, because both are built from the same ^{234}Th literature. Dropping it leaves the coefficient unchanged in sign and strength (n = 3,592, z_slope = +0.070, $P = 5.7 \times 10^{-22}$). It dilutes the estimate slightly rather than supporting it, and is retained only for completeness.

A fourth compilation, a global sediment-trap synthesis[24] (14,055 records), was assembled and screened but carries neither response variable. It enters no model and is not used further.

Co-location radius 3° with 1–5° sensitivity analysis (Fig. 4b): the e-ratio coefficient is stable from 1° (+0.103, n = 5,186) through 3° (+0.073, n = 6,539); no further stations enter at 5°.

Regressions

All predictors were z-standardized. The E1 (e-ratio) model used logit(e-ratio) with dFe and a slope × dFe interaction. The E2 (POC/^{234}Th) model controlled log sampling depth and export pathway.

Robustness: station–day block bootstrap (8,848 blocks; 2,000 replicates); Longhurst-province fixed effects with province-clustered errors; temporal-window restriction |lag| ≤ 2 years; radius sensitivity. Macro-segment significance in the HC3 model (−0.031, P = 0.0013) crosses zero under block bootstrapping and is reported as non-robust.

Heatwave and fishing stripping

NOAA OISST v2.1 monthly means[20,21] (1982–2025; 0.25°, complete global download) were extracted for 430 valid ocean cells. SST trend was computed by OLS per cell (mean +0.25 °C decade^{-1}).

Marine heatwave exposure used the Hobday fixed-baseline definition[10] (1982–2011, 90th percentile), scored as mean annual above-threshold months over 2015–2025 (0.2–10.1). A self-referential baseline is mathematically degenerate (constant 1.2 months) and was rejected *a priori*. Pre-sampling five-year SST anomaly completed the thermal set.

Fishing: cells were assigned EEZs via MarineRegions WFS point-in-bbox attribute queries (267 cells matched; 366 high-seas cells carried an indicator), and Sea Around Us catch statistics (1980–2019)[11] provided log catch level and OLS log-trend per fishing entity.

Nested models B0–B4 were fit on identical samples (B1/B3 restricted to heatwave-valid cells, n = 2,418); B4 aggregates to station means (n = 384).

2050 projection

Bio-ORACLE ERDDAP served SSP2-4.5 and SSP5-8.5 2020–2100 mean layers (six variables, 0.5° surface). 2050s fields (time index 3) were matched to analysis cells by cKDTree nearest neighbour; SSP grids are 0.25°-derived and require explicit re-matching.

The C1 meso-slope predictor (SST + $\log_{10}$ dFe + O_2) produces Δslope, which propagates through the C2 coupling with coefficient-covariance resampling (200 draws) to a distribution of ΔPOC/^{234}Th per cell. Failure is pre-defined as >15% decline.

Scenario similarity was verified against the forcing fields (ΔSST 0.06 °C; ΔdFe 0.2%) and is not a pipeline artefact.

Declarations

Data and code availability

All datasets are public (PANGAEA, Bio-ORACLE ERDDAP, GEOTRACES/BODC, OSU VGPM, NOAA OISST, Sea Around Us, MarineRegions). Analysis code and derived tables are archived on Zenodo.

Acknowledgements

No funding was received for this research.

Author contributions

Ning Zhou designed the study, performed the analyses and wrote the manuscript.

Competing interests

The author declares no competing interests.

References

1. Daufresne, M., Lengfellner, K. & Sommer, U. Global warming benefits the small in aquatic ecosystems. *Proc. Natl Acad. Sci. USA***106**, 12788–12793 (2009). https://doi.org/10.1073/pnas.0902080106
2. Armstrong, R. A., Lee, C., Hedges, J. I., Honjo, S. & Wakeham, S. G. A new, mechanistic model for organic carbon fluxes in the ocean based on the quantitative association of POC with ballast minerals. *Deep-Sea Res. II***49**, 219–236 (2002). https://doi.org/10.1016/S0967-0645(01)00101-1
3. Guidi, L. et al. Effects of phytoplankton community on production, size, and export of large aggregates: a world-ocean analysis. *Limnol. Oceanogr.***54**, 1951–1963 (2009). https://doi.org/10.4319/lo.2009.54.6.1951
4. Ward, B. A., Dutkiewicz, S., Jahn, O. & Follows, M. J. A size-structured food-web model for the global ocean. *Limnol. Oceanogr.***57**, 1877–1891 (2012). https://doi.org/10.4319/lo.2012.57.6.1877
5. Serra-Pompei, C., Soudijn, F. H., Visser, A. W., Kiørboe, T. & Andersen, K. H. A general size- and trait-based model of plankton communities. *Prog. Oceanogr.***189**, 102473 (2020). https://doi.org/10.1016/j.pocean.2020.102473
6. Negrete-García, G. et al. Plankton energy flows using a global size-structured and trait-based model. *Prog. Oceanogr.***209**, 102898 (2022). https://doi.org/10.1016/j.pocean.2022.102898
7. Richardson, T. L. & Jackson, G. A. Small phytoplankton and carbon export from the surface ocean. *Science***315**, 838–840 (2007). https://doi.org/10.1126/science.1133471
8. Henson, S. A., Sanders, R. & Madsen, E. Global patterns in efficiency of particulate organic carbon export and transfer to the deep ocean. *Glob. Biogeochem. Cycles***26**, GB1028 (2012). https://doi.org/10.1029/2011GB004099
9. Guidi, L. et al. Plankton networks driving carbon export in the oligotrophic ocean. *Nature***532**, 465–470 (2016). https://doi.org/10.1038/nature16942
10. Hobday, A. J. et al. A hierarchical approach to defining marine heatwaves. *Prog. Oceanogr.***141**, 227–238 (2016). https://doi.org/10.1016/j.pocean.2015.12.014
11. Pauly, D. & Zeller, D. Catch reconstructions reveal that global marine fisheries catches are higher than reported and declining. *Nat. Commun.***7**, 10244 (2016). https://doi.org/10.1038/ncomms10244
12. Kiko, R. et al. A global marine particle size distribution dataset obtained with the Underwater Vision Profiler 5. *Earth Syst. Sci. Data***14**, 4315–4337 (2022). https://doi.org/10.5194/essd-14-4315-2022
13. Picheral, M. et al. The Underwater Vision Profiler 5: an advanced instrument for high spatial resolution studies of particle size spectra and zooplankton distribution. *Limnol. Oceanogr. Methods***8**,

462–473 (2010). https://doi.org/10.4319/lom.2010.8.462

14. Assis, J. et al. Bio-ORACLE v3.0: pushing marine data layers to the CMIP6 Earth system models of climate change research. *Glob. Ecol. Biogeogr.***33**, e13813 (2024). https://doi.org/10.1111/geb.13813
15. Le Moigne, F. A. C., Henson, S. A., Sanders, R. J. & Madsen, E. Global database of surface ocean particulate organic carbon export fluxes diagnosed from the ^{234}Th technique. *Earth Syst. Sci. Data***5**, 295–304 (2013). https://doi.org/10.5194/essd-5-295-2013
16. Puigcorbé, V. Global database of oceanic particulate organic carbon to particulate ^{234}Th ratios [dataset]. *PANGAEA* (2019). https://doi.org/10.1594/PANGAEA.911423
17. Melgar-González, L., González-González, B., Baumas, C. M. J. & Villa-Alfageme, M. Global particulate organic carbon flux derived from Th-234: 13 ocean regions, 3 export depths [dataset]. *PANGAEA* (2026). https://doi.org/10.1594/PANGAEA.986750
18. Schlitzer, R. et al. The GEOTRACES Intermediate Data Product 2017. *Chem. Geol.***493**, 210–223 (2018). https://doi.org/10.1016/j.chemgeo.2018.05.040
19. GEOTRACES Intermediate Data Product Group. The GEOTRACES Intermediate Data Product 2025 (IDP2025) [dataset]. British Oceanographic Data Centre (2025). https://doi.org/10.5285/42c92148-8d03-8be6-e063-7086abc09f0c
20. Reynolds, R. W. et al. Daily high-resolution-blended analyses for sea surface temperature. *J. Clim.***20**, 5473–5496 (2007). https://doi.org/10.1175/2007JCLI1824.1
21. Huang, B. et al. Improvements of the Daily Optimum Interpolation Sea Surface Temperature (DOISST) version 2.1. *J. Clim.***34**, 2923–2939 (2021). https://doi.org/10.1175/JCLI-D-20-0166.1
22. Buesseler, K. O. & Boyd, P. W. Shedding light on processes that control particle export and flux attenuation in the twilight zone of the open ocean. *Limnol. Oceanogr.***54**, 1210–1232 (2009). https://doi.org/10.4319/lo.2009.54.4.1210
23. Behrenfeld, M. J. & Falkowski, P. G. Photosynthetic rates derived from satellite-based chlorophyll concentration. Limnol. Oceanogr. 42, 1–20 (1997). https://doi.org/10.4319/lo.1997.42.1.0001
24. Mouw, C. B., Barnett, A. B., McKinley, G. A., Gloege, L. & Pilcher, D. J. Global ocean particulate organic carbon flux merged with satellite parameters. *Earth Syst. Sci. Data***8**, 531–541 (2016). https://doi.org/10.5194/essd-8-531-2016

Figures

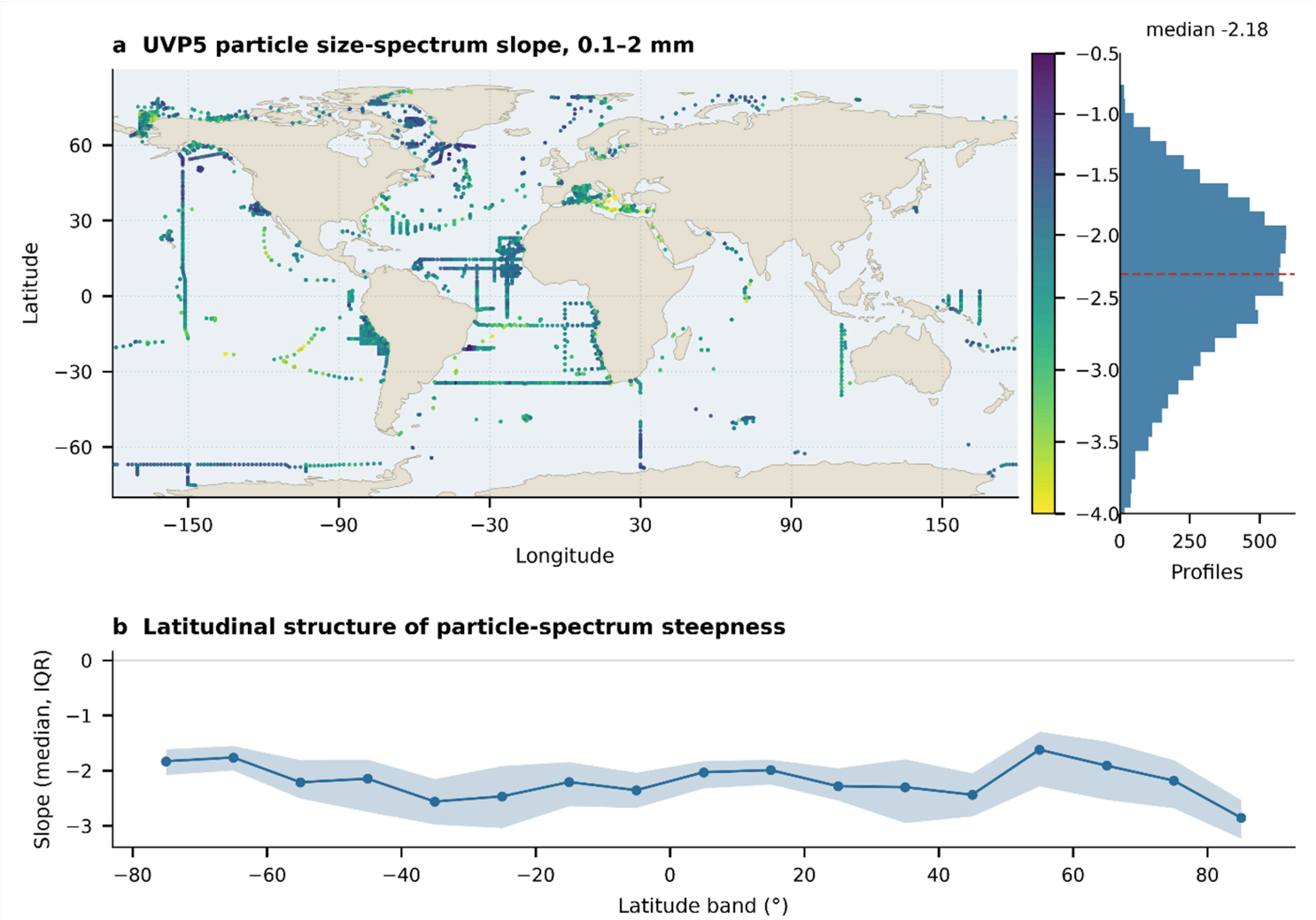


Figure 1

Global particle size-spectrum slopes. (a) Mesoplankton (0.1–2 mm ESD) particle size-spectrum slope from 8,479 UVP5 profiles (137 cruises, 75°S–81°N); more negative values indicate steeper spectra. (b) Co-located environmental drivers (Bio-ORACLE v3, 0.5°).

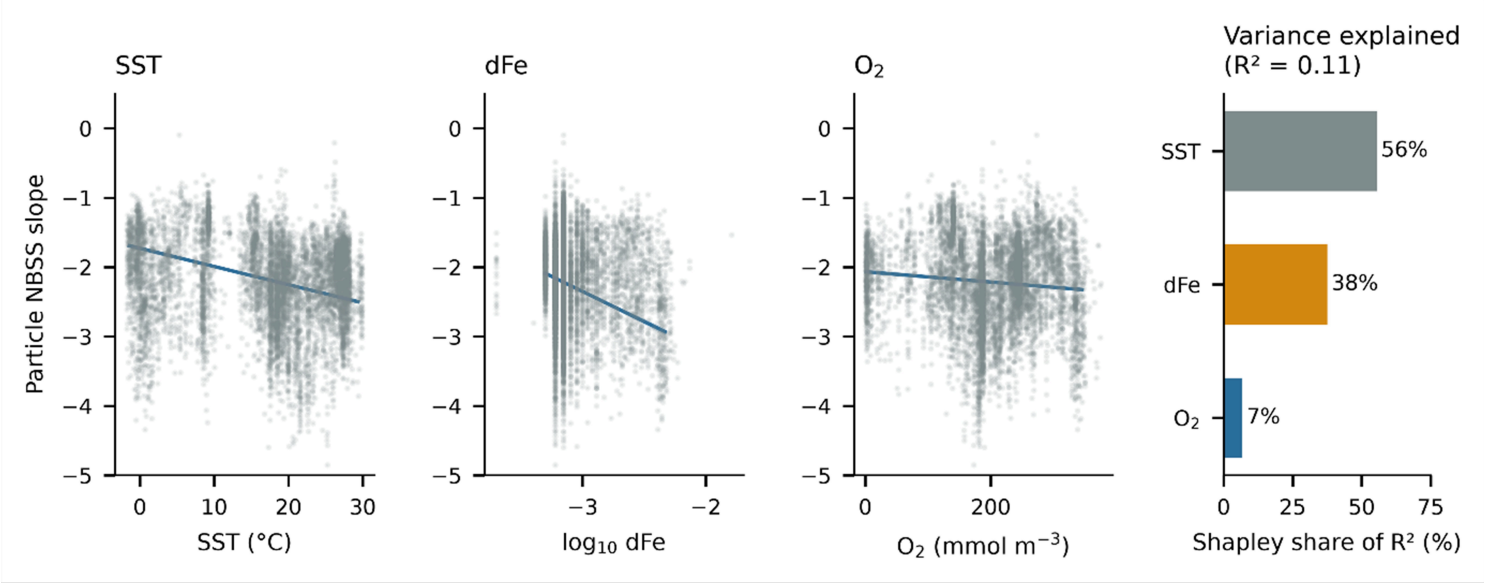


Figure 2

Driver elasticities of the mesoplankton spectrum slope. Standardized coefficients with 95% CIs and Shapley variance shares (SST 55.6%, log dFe 37.6%, O_2 6.9%) from the *n* = 8,479-profile model; inset: latitude-band medians.

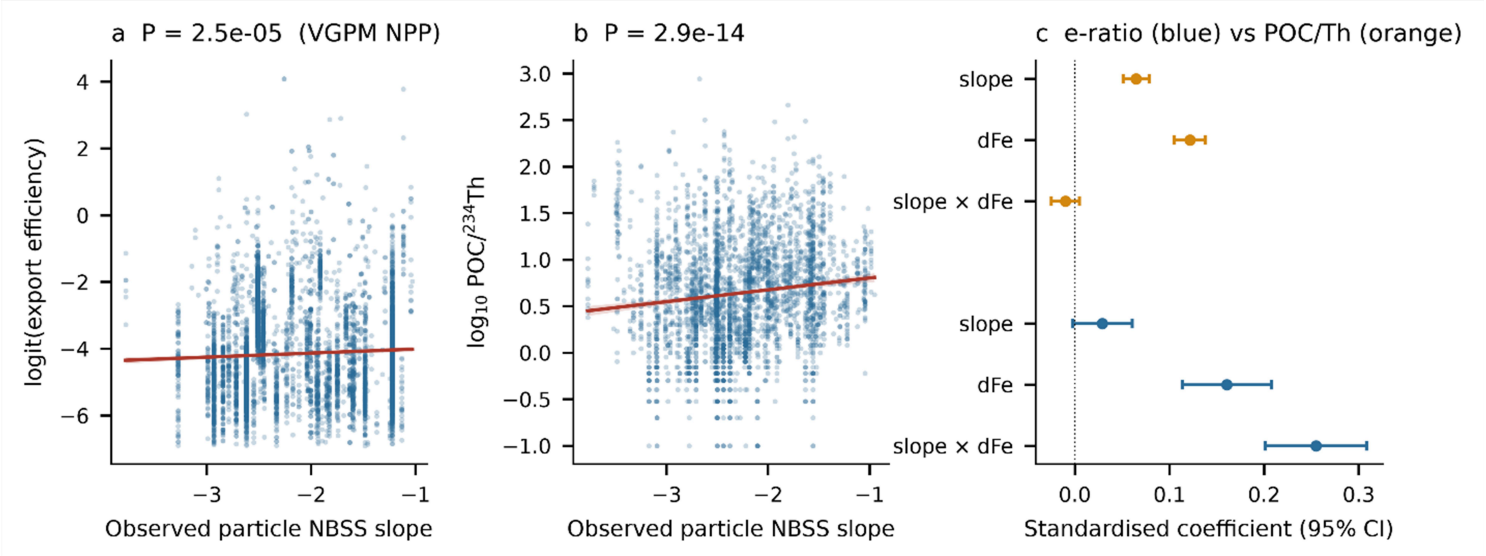


Figure 3

Size-spectrum slope versus particle export. (a) logit e-ratio versus slope, *n* = 6,539 co-located records (VGPM NPP basis); coefficient +0.073 per SD, $P = 2.5 \times 10^{-5}$. (b) $\log_{10}$ POC/^{234}Th versus slope, *n* = 3,680 co-located records; bivariate coefficient +0.070 per SD (+0.127 per unit slope), $P = 8.7 \times 10^{-14}$; the +0.065 coefficient is from the full model controlling log depth and pathway. (c) Standardized coefficients of the E1/E2 models.

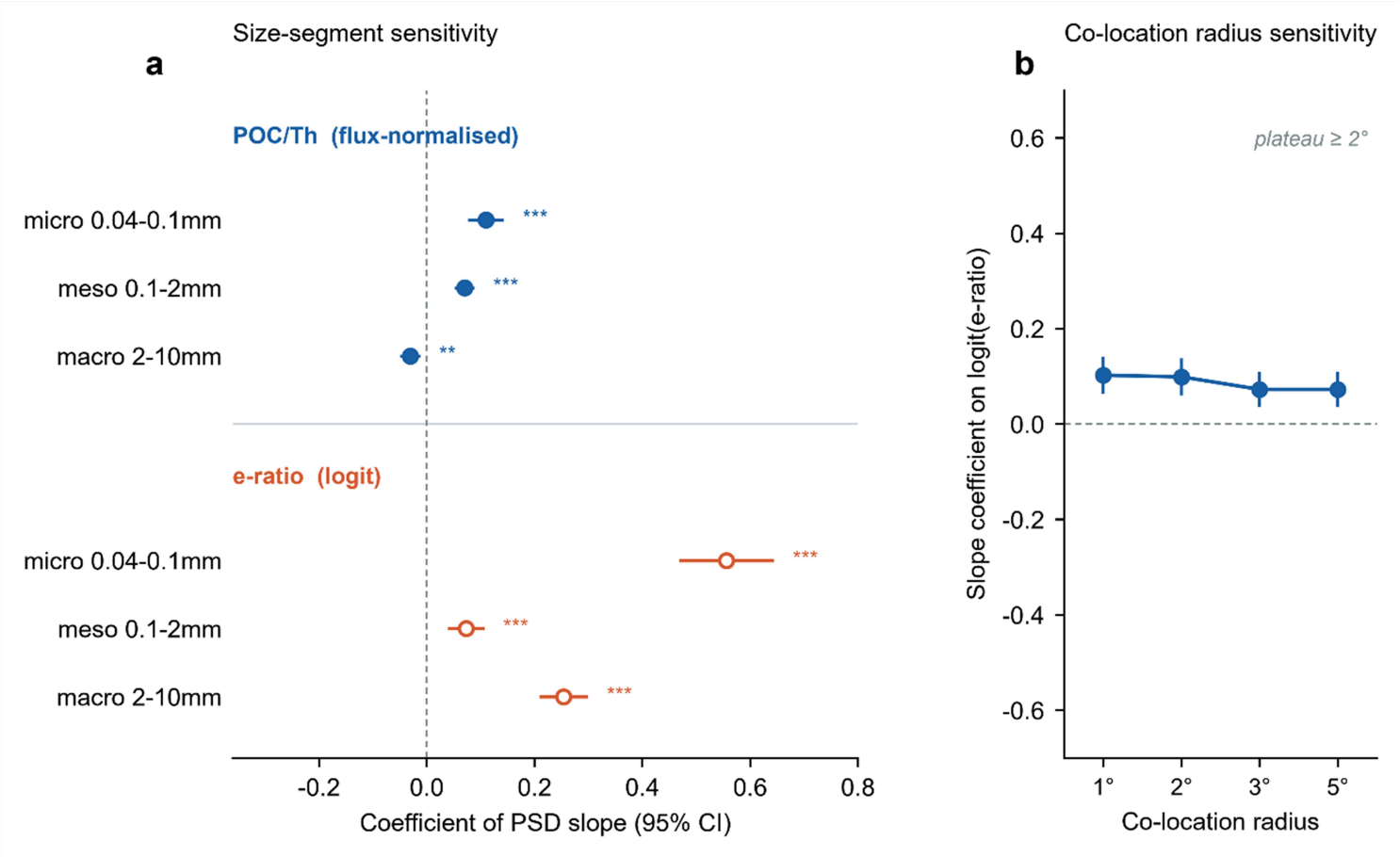


Figure 4

Robustness and segmentation. (a) Slope–export coefficients by size segment: POC/^{234}Th micro 0.04–0.1 mm (*n* = 606), meso 0.1–2 mm (*n* = 3,680), macro 2–10 mm (*n* = 3,480); e-ratio micro (*n* = 1,429), meso (*n* = 6,539), macro (*n* = 5,057). (b) e-ratio co-location radius sensitivity: *n* = 5,186, 5,818, 6,539, 6,539 at 1°, 2°, 3°, 5°. (c) Block bootstrap and Longhurst-province distributions. (d) Nested confounder-stripping models B0–B4 (baseline +0.0649; retention 109% / 82% / 97%; station-mean *n* = 384, retention 101%).

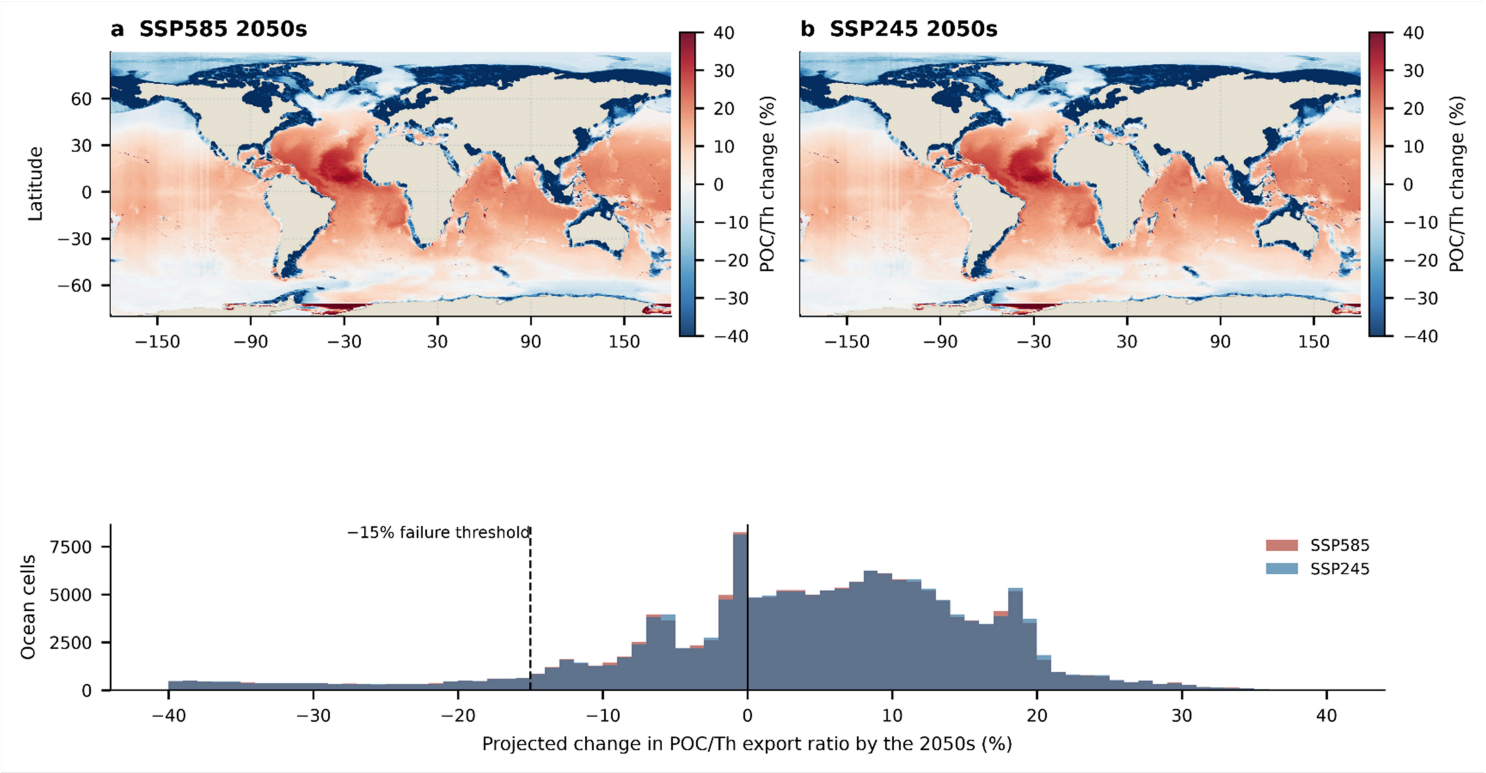


Figure 5

Projected 2050s change in POC/^{234}Th. (a, b) Median projected change in POC/^{234}Th versus the 2000–2019 baseline across 200 coefficient-covariance draws under SSP5-8.5 (a) and SSP2-4.5 (b); failure (>15% decline) covers 14% of ocean cells and gain (>15%) 17% under both scenarios, which are near-identical at mid-century (ΔSST 0.06 °C). Bottom: distribution across ocean cells with the −15% failure threshold (dashed line).